



1 **Evaluation of UV-visible MAX-DOAS aerosol profiling**
2 **products by comparison with ceilometer, sun photometer,**
3 **and in situ observations in Vienna, Austria**

4 **Stefan F. Schreier¹, Tim Bösch², Andreas Richter², Kezia Lange², Michael Revesz¹,**
5 **Philipp Weihs¹, Mihalis Vrekoussis^{2,3}, and Christoph Lotteraner⁴**

6 ¹Institute of Meteorology and Climatology, University of Natural Resources and Life Sciences,
7 Vienna, Austria

8 ²Institute of Environmental Physics, University of Bremen, Germany

9 ³Climate and Atmosphere Research Center (CARE-C), The Cyprus Institute, Cyprus

10 ⁴Central Institute for Meteorology and Geodynamics, Vienna, Austria

11 Correspondence to: S. F. Schreier (stefan.schreier@boku.ac.at)

12

13 **Abstract**

14 Since May 2017 and August 2018, two ground-based MAX-DOAS (Multi AXis Differential
15 Optical Absorption Spectroscopy) instruments have been continuously recording daytime spectral
16 UV-visible measurements in the north-west (University of Natural Resources and Life Sciences
17 (BOKU) site) and south (Arsenal site) of the Vienna city centre (Austria), respectively. In this
18 study, aerosol extinction (AE) profiles, aerosol optical depth (AOD), and near-surface AE are
19 retrieved from MAX-DOAS measurements recorded on cloud-free days applying the Bremen
20 Optimal estimation REtrieval for Aerosols and trace gasS (BOREAS) algorithm. For the first time,
21 measurements of atmospheric profiles of pressure and temperature obtained from routinely
22 performed sonde ascents are used to calculate box-air-mass-factors and weighting functions for
23 different seasons. The performance of BOREAS was evaluated against co-located ceilometer, sun
24 photometer, and in situ instrument observations covering all four seasons. The results showed that
25 the vertical AE profiles retrieved from the BOKU UV-visible MAX-DOAS observations are in
26 very good agreement with data from the co-located ceilometer, reaching correlation coefficients



1 (R) of 0.91-0.99 (UV) and 0.85-0.98 (visible) during fall, winter, and spring seasons. Moreover,
2 AE extracted using the lowest part of MAX-DOAS vertical profiles (up to 100 m above ground)
3 are highly consistent with near-surface ceilometer AE ($R > 0.90$ and linear regression slopes of
4 ~ 0.90) during the fall season. A strong correlation is also found for the BOREAS-based AODs
5 when compared to the AERONET ones. Notably, the highest correlation coefficients ($R = 0.95$ and
6 $R = 0.94$ for UV and visible, respectively) were identified for the fall season. While high correlation
7 coefficients are also found for the winter and spring seasons, the results are less reliable for
8 measurements taken during summer. For the first time, the spatial variability of AOD and near-
9 surface AE over the urban environment of Vienna is assessed by analyzing the retrieved and
10 evaluated BOREAS aerosol profiling products in terms of different azimuth angles of the two
11 MAX-DOAS instruments and for different seasons. We found that the relative differences of
12 averaged AOD between different azimuth angles are 7-13%, depending on the season. Larger
13 relative differences of up to 32% obtained for the different azimuthal directions are found for near-
14 surface AE. This study revealed the strong capability of BOREAS to retrieve AE profiles, AOD,
15 and near-surface AE over urban environments and demonstrated its use for identifying the spatial
16 variability of aerosols, in addition to the temporal variation.

17

18 **1 Introduction**

19 Atmospheric aerosols are defined as particles (liquid or solid) suspended in the air, with particle
20 diameters in the range of 10^{-9} to 10^{-4} m (0.001 μm to 100 μm) and various shapes, chemical
21 compositions, and hygroscopic and optical properties (Seinfeld and Pandis, 2006). Aerosols are an
22 important component of the Earth's atmosphere and play a crucial role in atmospheric chemistry,
23 cloud formation and lifetime, Earth's radiation budget, and climate (IPCC, 2013). It has also been
24 widely documented that enhanced atmospheric aerosol loading has adverse effects on human health
25 (Lelieveld et al., 2015).

26 Sources of aerosols include natural emissions from the sea surface, soils, terrestrial vegetation,
27 volcanoes, and wildfires as well as anthropogenic emissions from agricultural and industrial
28 activities, combustion processes, abrasion, and solvent use (Kanakidou et al., 2018).



1 A number of instruments for ground-based observations have been developed in the last decades
2 to obtain aerosol optical properties and vertical profiles in the troposphere. In situ instruments (e.g.
3 optical particle counters) are often designed to measure particulate matter (PM) concentrations (e.g.
4 PM_{2.5} and PM₁₀, whose size is defined as less than 2.5 and 10 μm in diameter, respectively) in
5 ambient air.

6 In addition to in situ measurement techniques, ground-based remote sensing instruments such as
7 sun photometers, Light Detection And Ranging (LIDAR), ceilometers, and Multi AXis Differential
8 Optical Absorption Spectrometers (MAX-DOAS) as well as corresponding retrieval approaches
9 have been developed to obtain aerosol optical properties and vertical profiles (Holben et al., 1998;
10 Ansmann et al., 2011; Madonna et al., 2018; Frieß et al., 2016).

11 From sun photometer measurements, precise information on the total aerosol extinction (AE) and
12 scattering phase function can be derived and column-averaged aerosol size distribution, single
13 scattering albedo, and refractive index can be extracted (Holben et al., 1998).

14 Research grade LIDARs provide vertical profiles of aerosol backscattering and other information
15 at high vertical resolution (e.g. Madonna et al., 2018). In contrast, the retrieval of attenuated
16 backscatter and aerosol backscattering coefficient from ceilometer observations is limited by
17 instrument accuracy and highly dependent on the availability of data from co-located ancillary
18 instruments (e.g. sun photometer and/or Raman multi-wavelength LIDAR). However, the lower
19 costs and lower maintenance requirements associated with commercial ceilometers make these
20 instruments attractive for ground-based observations of aerosol optical properties and vertical
21 profiles in global scale networks (Madonna et al., 2018; Lotteraner and Piringer, 2016; Baumann-
22 Stanzer et al., 2019).

23 More than 15 years ago, a method to derive aerosol optical properties and vertical profiles from
24 MAX-DOAS observations was presented (Wagner et al., 2004), and since then has received
25 increasing attention (e.g. Frieß et al., 2006; Clémer et al., 2010; Yilmaz, 2012; Wang et al., 2013;
26 Vlemmix et al., 2015; Chan et al., 2017; Bösch et al., 2018; Beirle et al., 2019; Friedrich et al.,
27 2019). The derived aerosol information has been used for environmental studies as well as for the
28 validation of satellite observations and model simulations (e.g. Ma et al., 2013). State-of-the-art
29 MAX-DOAS retrieval algorithms (Tirpitz et al., 2020 and references therein) can be used to



1 quantify horizontal inhomogeneities in aerosol loading over urban and rural areas, in addition to
2 the aerosol vertical distribution. Further research efforts are needed to better retrieve aerosol optical
3 properties and vertical profiles by using the above mentioned algorithms and to compare and
4 validate the resulting aerosol products against independent co-located measurements.

5 In this study, we evaluate and analyze AE profiles, aerosol optical depth (AOD), and near-surface
6 (e.g. the lowest extinction point representing the altitude range between the surface and up to 100
7 m) AE retrieved from UV-visible spectral measurements collected with two MAX-DOAS
8 instruments in Vienna, Austria, located in the north-west and south of the city center. The retrieval
9 of UV-visible aerosol profiling products is based on the BOREAS algorithm (Bremen Optimal
10 estimation REtrieval for Aerosols and trace gaseS) (Bösch et al., 2018), which has been developed
11 by the Institute of Environmental Physics of University of Bremen (IUP-B) to improve an earlier
12 profile retrieval algorithm (Wittrock, 2006). The retrieval performance of BOREAS was recently
13 assessed from synthetic data computed with SCIATRAN (Rozanov et al., 2014) as well as using
14 real-world measurements taken in September 2016 during the Second Cabauw Intercomparison
15 campaign for Nitrogen Dioxide measuring Instruments (CINDI-2) in a rural environment (Frieß et
16 al., 2019; Tirpitz et al., 2020). From spectral measurements collected during CINDI-2, AE profiles
17 and AOD retrieved with BOREAS were validated with ancillary data. Overall, the results show a
18 satisfactory performance of BOREAS when the retrieved synthetic profile is close to the a priori.
19 However, due to the coarse vertical resolution (100 m), a comparison with surface in situ
20 measurements remains challenging. More recently, Gratsea et al. (2020) reported on the BOREAS
21 retrieval of AE profiles from ground-based MAX-DOAS measurements taken over the urban
22 environment of Athens, Greece. For validation purposes, they selected four case studies covering
23 different seasons and origins of aerosol loads and assessed the performance of BOREAS through
24 comparison with ground-based lidar AE profiles and sun photometer AOD measurements.

25 This study aims to evaluate UV-visible aerosol profiling products retrieved with BOREAS, in this
26 case over the urban environment of Vienna, Austria, through comparison with co-located
27 instruments. In a first step, AE profiles, AOD, and near-surface AE are retrieved from MAX-DOAS
28 UV and visible spectral measurements conducted on the roof of a campus building of the University
29 of Natural Resources and Life Sciences (BOKU) on cloud-free days in the period between
30 September 2017 and August 2019. The BOREAS aerosol profiling products are then compared



1 with data from co-located ceilometer, sun photometer, and in situ instruments. In the second step,
2 additional insights into the spatio-temporal variability of AOD and near-surface AE over the urban
3 environment of Vienna are provided by analyzing BOREAS aerosol profiling products retrieved
4 from measurements collected with two MAX-DOAS instruments (BOKU and Arsenal). By
5 plotting AOD and near-surface AE against simultaneous BOREAS retrievals of tropospheric
6 nitrogen dioxide vertical column densities (NO₂ VCDs) and near-surface NO₂, respectively, the
7 origin of the aerosol is discussed.

8 The paper is structured as follows: in section 2, the instruments used in this study and the respective
9 data retrievals/data products are presented. As the study is based on cloud-free days, the
10 methodology to select such days is also introduced in this section. Results and insights into the
11 spatial and temporal patterns and the origin of aerosols over the urban environment of Vienna are
12 presented in section 3, followed by a summary and conclusions (section 4).

13

14 **2 Methodology**

15 **2.1 Instrumentation**

16 **2.1.1 MAX-DOAS**

17 Within the framework of the VINDOBONA (VIenna horizontal aNd vertical Distribution
18 OBServations Of Nitrogen dioxide and Aerosols) project, three ground-based MAX-DOAS
19 instruments have been assembled and put in continuous operation since December 2016, May
20 2017, and August 2018 at three different locations in Vienna (www.doas-vindobona.at). As the
21 lowest elevation angles which are essential for the retrieval of AE profiles are partially blocked by
22 trees and buildings at the University of Veterinary Medicine (VETMED) site, measurements of the
23 third MAX-DOAS instrument are not considered in this study.

24 Briefly, MAX-DOAS is a ground-based remote sensing technique for retrieving tropospheric trace
25 gases and aerosols by measuring scattered sunlight at different azimuthal and elevation angles (e.g.
26 Wagner et al., 2004). The MAX-DOAS systems measuring in Vienna were developed at the
27 Institute of Environmental Physics of the University of Bremen (IUP-B) in Bremen, Germany (e.g.



1 Peters, 2013) and continuously improved during international measurement campaigns such as
2 CINDI, TransBrom, SHIVA, MAD-CAT, and CINDI-2 (Roscoe et al., 2010; Peters et al., 2012;
3 Schreier et al., 2015; Wang et al., 2017; Donner et al., 2019). After the assembly, characterization
4 and testing phases in the laboratory of IUP-B, these instruments were transferred to the locations
5 in Vienna, where they continuously measure scattered sunlight at selected azimuthal and elevation
6 angles to cover air masses over large parts of the urban environment (Schreier et al., 2020).

7 In this study, UV-visible spectral measurements are taken from the BOKU and Arsenal MAX-
8 DOAS instruments located in the north-west (48.2379°N, 16.3317°E, 267 m a.s.l.) and south
9 (48.1818°N, 16.3908°E, 333 m a.s.l.) of the city center, respectively (see Fig. 1 and Table 1). The
10 two instruments are operating in two configurations: (1) elevation scans at fixed azimuthal
11 directions and (2) azimuthal scans at fixed elevation angles. The former configuration, which is
12 considered in this study, is based on five azimuthal viewing directions between 74° and 144°
13 (BOKU MAX-DOAS) and six azimuthal viewing directions between 324° and 20° (Arsenal MAX-
14 DOAS) (see Fig. 1), which were selected to capture the city center as well as point into the direction
15 of the other MAX-DOAS instruments. Elevation sequences consisting of $\alpha = 0^\circ, 1^\circ, 2^\circ, 3^\circ, 4^\circ, 5^\circ,$
16 $10^\circ, 15^\circ, 30^\circ,$ and 90° (zenith) are continuously performed at these azimuthal directions. Further
17 technical details about the spectrometers of the BOKU (Shamrock SR-193i-A) and Arsenal
18 (AvaSpec-ULS2048x64) MAX-DOAS instruments can be found in Schreier et al. (2020) and
19 Behrens et al. (2019), respectively.

20

21 **2.1.2 Ceilometer**

22 The national weather service in Austria, “Zentralanstalt für Meteorologie und Geodynamik”
23 (ZAMG), operates a commercial ceilometer of the type Vaisala CL51 at the site “Hohe Warte”
24 (48.2483°N, 16.3564°E, 198 m a.s.l.) of ZAMG (see Fig. 1 and Table 1), performing routine
25 measurements since July 2012 (Lotteraner and Piringer, 2016). Briefly, the Vaisala CL51
26 ceilometer (hereinafter referred to as ceilometer) uses diode-laser lidar technology that emits
27 powerful laser pulses with wavelengths of 910 ± 10 nm in a vertical direction. Backscatter signals
28 are collected from about 50 m above ground up to an altitude of 15 km with a vertical resolution
29 of 10 m (Wagner and Schäfer, 2015). Recently, a method to obtain time series of mixing-heights



1 from ceilometer measurements was developed at ZAMG (Lotteraner and Piringer, 2016). In our
2 study, backscatter profiles with a temporal resolution of about half a minute are converted into AE
3 profiles (see section 2.2.3), which are used to evaluate AE profiles retrieved with BOREAS (see
4 section 3.1.1).

5

6 **2.1.3 Sun photometer**

7 Since May 2016, the Institute of Meteorology and Climatology of BOKU (BOKU-Met) operates a
8 sun photometer (Cimel CE318) within the AERONET (AErosol RObotic NETwork) project
9 (<https://aeronet.gsfc.nasa.gov/>). Briefly, the ground-based Cimel CE318 sun photometer
10 (hereinafter referred to as sun photometer) measures direct sunlight at different and selected
11 wavelength ranges. The extinction measurements are used to calculate column-integrated AODs
12 and Angstrom exponents (Holben et al., 1998). Additionally, column-integrated aerosol parameters
13 such as size distribution, refractive index, single scattering albedo, and phase function can be
14 retrieved by applying AERONET Version 3 inversion algorithms. The sun photometer is located
15 on the BOKU-Met measurement platform at a distance of about 2.5 m from the BOKU MAX-
16 DOAS instrument (see Fig. 1 and Table 1). In this study, AOD at 340, 380, 440, 500, 870, and
17 1020 nm are used for the scaling of ceilometer backscatter profiles (see section 2.2.3) as well as
18 for the comparison with AOD retrieved from BOKU MAX-DOAS UV-visible spectral
19 measurements (see section 3.1.2).

20

21 **2.1.4 In situ**

22 The Vienna air quality monitoring network, which is maintained by the “Wiener
23 Umweltschutzabteilung (Magistratsabteilung 22)”, provides continuous half-hourly values of
24 PM_{2.5} and PM₁₀ from six and thirteen, respectively, in situ instruments (e.g. Grimm EDM180)
25 within the boundaries of Vienna (<https://www.wien.gv.at/ma22-lgb/luftgi.htm>). In this study,
26 PM₁₀ data are obtained from the station “Gerichtsgasse” (48.2611°N, 16.3969°E, 164 m a.s.l.)
27 located in Vienna’s 21st district “Floridsdorf” (see Fig. 1), which is a site characteristic for the
28 urban background and located close to the 74° azimuthal viewing direction of the BOKU MAX-



1 DOAS. These measurements, which have been continuously performed since January 2017 using
2 a Grimm EDM180 (Spangl, 2019), are used for the comparison of MAX-DOAS retrieved near-
3 surface AE (see section 3.1.3).

4

5 **2.2 Data retrieval and analysis**

6 **2.2.1 Selection of days with cloud-free conditions**

7 The evaluation of UV-visible MAX-DOAS aerosol profiling products in this study is based on days
8 with cloud-free conditions. To select the cloud-free days in Vienna, the following procedure is
9 applied:

10 First, clear sky global radiation for the period September 2017 to August 2019 is simulated using
11 the radiative transfer (RTM) solver DISORT2 (Stamnes et al., 1988) of the radiative transfer
12 software package libRadtran (Mayer and Kylling, 2005). Mean vertical atmospheric profiles (mid-
13 latitude summer and winter as a function of the season) are used as input parameters for the RTM
14 calculations. Column ozone is taken from the routine measurements from satellite data base at the
15 WOUDC (woudc.org), solar zenith angle (SZA) is taken from retrieved MAX-DOAS data, and
16 AOD is taken from AERONET. Hence, the temporal resolution of the simulated global radiation
17 matches the MAX-DOAS retrieved differential slant column densities (DSCDs).

18 Second, the simulated and measured global radiation is compared to pre-select cloud-free days.
19 The measured global radiation in this study is obtained from star pyranometer (Schenk)
20 observations, which are performed since the year 2005 at the BOKU-Met measurement platform
21 as part of the BOKU-Met weather station (<https://meteo.boku.ac.at/wetter/aktuell/>). Briefly, the
22 Schenk star pyranometer has six black and six white painted sectors, whereby the temperature
23 difference between the black and white segments is proportional to the incident solar radiation. For
24 this comparison, the measured global radiation is temporally resampled to the MAX-DOAS time
25 series.

26 In the third step, the following criteria are used to select cloud-free days: (i) data points are defined
27 as “low error” if the difference between measured and simulated global radiation, relative to the



1 simulated global radiation, is below or equal to 20%, (ii) for a day to be considered as clear or
2 partially clear sky at least 60% of the data points must be classified as “low error”, and (iii) the
3 daily sum of the second-order difference is used as a measure of sky condition variability. The daily
4 total second-order difference of the measured data must be less than 2.5 times the one of the
5 simulated data. The value 2.5 was found to work best for the separation between clear and cloudy
6 skies in our case. The above criteria were found by trial-and-error. Due to the annual variation of
7 radiation there can not be a single empirically determined criteria. After applying these criteria, a
8 total number of 119 days from September 2017 to August 2019 remains. However, the final number
9 of cloud-free days used in this study is further reduced due to missing MAX-DOAS and/or
10 ceilometer and/or sun photometer and/or atmospheric sounding observations. Thus, total numbers
11 of 102 cloud-free days (40 days in fall, 14 days in winter, 22 days in spring, and 28 days in summer)
12 for the BOKU UV, 74 cloud-free days (27 days in fall, 10 days in winter, 9 days in spring, and 28
13 days in summer) for the BOKU visible, and 81 cloud-free days (27 days in fall, 10 days in winter,
14 16 days in spring, and 28 days in summer) for the Arsenal MAX-DOAS instruments are selected
15 for the retrieval of vertical AE profiles, AOD, and near-surface AE. It should be noted that the total
16 number of days with cloud-free conditions is lower for the BOKU visible and Arsenal MAX-DOAS
17 because their operation started later in time and also because of technical problems with the BOKU
18 visible MAX-DOAS in spring 2019, which resulted in the loss of a couple of days.

19

20 **2.2.2 Vertical AE profiles, AOD, and near-surface AE from MAX-DOAS** 21 **measurements**

22 The retrieval of AE profiles, AOD, and near-surface AE on cloud-free days is performed with the
23 BOREAS algorithm (Bösch et al., 2018). Briefly, the abundance of the oxygen molecule (O_2) only
24 depends on pressure and temperature, and decreases exponentially with altitude. The concentration
25 of the oxygen dimer, often referred to as O_2 - O_2 collision complex (O_4), is proportional to the
26 squared O_2 concentration and thus, decreases also exponentially with altitude. The column amounts
27 of the latter (O_4) can be retrieved from DOAS measurements in the UV and visible wavelength
28 range because of its spectral absorption features (Wagner et al., 2004). In general, the BOREAS
29 aerosol retrieval algorithm, which is fully implemented within the radiative transfer model



1 SCIATRAN (Rozaovanov et al., 2014), uses the difference between modelled and measured O₄
2 differential slant optical thicknesses around the O₄ absorption bands at 360 and 477 nm to retrieve
3 AE profiles in an iterative Tikhonov regularization scheme (Rodgers, 2004). In more detail,
4 SCIATRAN is used for the computation of weighting functions, which are needed for the profile
5 inversion of aerosols (Bösch et al., 2018). In addition to the O₄ DSCDs, which are retrieved using
6 the retrieval settings given in Schreier et al. (2020), atmospheric sondes profiles of pressure and
7 temperature are used as input. In this study, aerosol profiling products are retrieved with BOREAS
8 for the first time using measured atmospheric profiles of pressure and temperature from a co-
9 located site, instead of using profiles from a U.S. Standard Atmosphere (Bösch et al., 2018; Gratsea
10 et al., 2020) or averaged profiles of O₃ sonde measurements (Tirpitz et al., 2020). Atmospheric
11 profiles of pressure and temperature used in this study are measured twice a day at the “Hohe
12 Warte” site of ZAMG (see Fig. 1), e.g. at 12 UTC and 0 UTC. For the BOREAS retrieval, pressure
13 and temperature profiles taken at 12 UTC, which are downloaded from a global data base
14 (<http://weather.uwyo.edu/upperair/sounding.html>), are used as input.

15 The radiative transfer calculations with SCIATRAN are performed using the aerosol phase function
16 and single scattering albedo of AERONET Version 3 (Almucantar Level 1.5 Inversion) data from
17 the instrument located at BOKU, selecting the data closest in time to the MAX-DOAS
18 measurement. The general configuration of BOREAS was used to retrieve AE values on a vertical
19 grid ranging from the station altitude up to 4 km, with a 100 m grid step altitude. The a priori profile
20 was chosen to be exponentially decreasing (AE surface value: 0.18, scale height: 1.25 km) with the
21 pre-scaling option introduced in Bösch et al. (2018) to cope with highly varying aerosol loads. The
22 period between AE profiles, AOD, and near-surface AE retrieved at recurring azimuth viewing
23 directions was about 35-45 min until March 2019; and 50-75 minutes since then because of the
24 added azimuthal viewing directions for the first configuration and full implementation of the
25 second configuration (see section 2.1.1).

26 Although BOREAS NO₂ profiling products are briefly addressed to investigate the origin of
27 aerosols over the urban environment of Vienna (see section 3.2), the main focus of this study is on
28 aerosol profiles. Accordingly, details on the NO₂ retrieval are omitted and the reader is referred to
29 Bösch et al. (2018) and Schreier et al. (2020).



1

2 **2.2.3 Vertical AE profiles from ceilometer measurements**

3 Range-corrected backscatter profiles (hereinafter referred to as backscatter profiles) from
4 ceilometer observations can be converted into AE profiles as recently reported in the context of the
5 validation of AE profiles retrieved from MAX-DOAS measurements (Bösch et al., 2018; Wagner
6 et al., 2020). In this study, we follow the approach described in Wagner et al. (2020) to obtain AE
7 profiles using the following procedure: In a first step, both time and backscatter profiles are
8 extracted from the original (daily) data files, which are made available by ZAMG. Second,
9 extremely high values (> 100000), which appear at altitudes well above the mixing-height, are
10 replaced with NaNs. The backscatter profiles are then vertically smoothed by applying a moving
11 average function in the third step. Fourth, the ceilometer profiles with higher temporal and vertical
12 resolution are aggregated to match both the time and altitude range of the MAX-DOAS AE profiles.
13 On the one hand, time assimilation is achieved by finding the ceilometer measurements closest in
14 time with the first MAX-DOAS measurements of individual vertical scans and then averaging the
15 backscatter signals. For the latter, data within a range of five values before the above time and
16 ending ten values after that time (~ 9.5 minutes, which is in good accordance with the duration of
17 one MAX-DOAS vertical scan) were used. As we use the first MAX-DOAS measurement of
18 individual vertical scans as time reference and because of the duration of several minutes of one
19 such scan, more values are used after that time reference. On the other hand, assimilation of vertical
20 resolution is achieved by averaging over intervals of ten backscatter signals (because of 10 m
21 vertical resolution) to match the 100 m vertical sampling of MAX-DOAS measurements. Once the
22 ceilometer measurements are assimilated to the time and vertical resolution of MAX-DOAS,
23 backscatter profiles are vertically integrated between the lowest (50 m above surface) and highest
24 altitude (4 km). The vertically integrated backscatter profiles are scaled in an intermediate step by
25 the AERONET AOD at 910 nm (average of AOD at 870 nm and 1020 nm) in order to match the
26 operating wavelength range of the ceilometer. Finally, the profiles are scaled by the AOD at 360
27 nm (average of AOD at 340 nm and 380 nm) and 470 nm (average of AOD at 440 nm and 500
28 nm), which is in accordance with MAX-DOAS AE profiles retrieved in the UV (Arsenal and
29 BOKU MAX-DOAS) and visible (BOKU MAX-DOAS only) spectral ranges (see Sect. 2.2.2),



1 respectively. We note that, in contrast to Wagner et al. (2020), an extinction correction is not
2 performed in our study because the effect of this correction was found to be negligible small.

3

4 **3 Results and discussion**

5 **3.1 Evaluation of BOREAS aerosol profiling products**

6 The performance of BOREAS in this study is evaluated by considering AE profiles, AOD, and
7 near-surface AE retrievals in the UV and visible channels that fulfill the following criteria: (1) the
8 absolute and relative difference between measured and simulated O_4 DSCDs is less than 1000
9 $\text{molec}^2 \text{cm}^{-5}$ and less than 10%, respectively, (2) the maximum AOD is less than 1.0, and (3) no
10 more than 50 iterations were needed in the retrieval. It should be noted that in some cases, the
11 absolute and relative difference criteria can be reached although no convergence of BOREAS is
12 found. In general, convergence is not reached if the a priori is not appropriate, for example when
13 the shape of the vertical profile and/or the assumed AOD are wrong. Moreover, temporal changes
14 in pressure and temperature can affect the BOREAS retrieval.

15

16 **3.1.1 Comparison of MAX-DOAS AE profiles with ceilometer AE profiles**

17 BOREAS AE profiles retrieved from the UV and visible BOKU MAX-DOAS measurements taken
18 at an azimuth angle of 74° (represented as a solid blue line in Fig. 1) are compared against AE
19 profiles obtained from the ceilometer, which is about 2.25 km away and close to the selected
20 viewing direction (see Fig. 1). The comparison is performed for all available cloud-free days falling
21 into the period September 2017 to August 2019 (see section 2.2.1) and presented for the different
22 seasons.

23 Overall, the MAX-DOAS AE profiles retrieved in the UV and visible range are consistent with
24 ceilometer AE profiles, in particular during the fall, winter, and spring seasons with correlation
25 coefficients of $R = 0.91\text{-}0.99$ (UV) and $R = 0.84\text{-}0.98$ (visible) (see Fig. 2 and Fig. 3, respectively).
26 In the left panels of that figures, all extinction points of MAX-DOAS and ceilometer extracted
27 from a number (N) of profiles available from cloud-free days within selected time intervals are



1 correlated with each other. Smaller R values are found for summer, with $R = 0.77-0.96$ (UV) and
2 $R = 0.46-0.96$ (visible). The largest correlation coefficients during summer are found in the early
3 morning (6-8 UTC), which could be related to the lower mixing-heights (< 1 km). Notably, higher
4 correlation coefficients are generally observed in the morning hours for both the UV and visible
5 channels and across all seasons. While the magnitudes of MAX-DOAS AE profiles below 2 km
6 altitude are mostly lower than those of the ceilometer data in the UV channel, better agreement of
7 the two independent retrievals is found for the visible channel. Note that the numbers of UV
8 retrievals differs from the number of visible retrievals, which can be explained by the different
9 length of time series (see section 2.2.1) and at the same time higher numbers of flagged retrievals
10 for the UV measurements (see section 3.1). The fact that the same number of cloud-free summer
11 days (28 days) are evaluated for the UV and visible BOREAS retrievals, but more BOREAS
12 retrievals are considered for the visible channel implies that more AE profile retrievals are flagged
13 as invalid in the UV channel. The reason for the higher correlation coefficients observed for the
14 UV profiles could be related to the fact that BOREAS AE profiles retrieved in the UV are probing
15 air masses closer to the MAX-DOAS instrument than the visible ones and are thus closer to the
16 ceilometer.

17 The right panels of Fig. 2 and Fig. 3 depict the comparison between MAX-DOAS and ceilometer
18 near-surface AE data, which is representative for the lowest level of the troposphere (e.g. from the
19 instrument's altitude up to 100 m above). In this case, the lowest extinction points from all daytime
20 measurements of available cloud-free days are correlated with each other. Consequently, the
21 number of data points is the sum of N of the five selected time spans given in the left panels plus
22 data points from time spans before and after the selected ones. The highest set of correlation
23 coefficients of $R > 0.90$ and linear regression slopes (S) of $S > 0.90$ are encountered in the fall
24 season, for both spectral channels. This finding implies that the BOREAS retrieval of near-surface
25 AE delivers the best results during that time of the year. These plots underline the difficulties that
26 BOREAS has in retrieving AE profiles and near-surface AE during summer, most probably due to
27 (i) well-mixed air masses as indicated by maximum mixing-heights, (ii) decreasing sensitivity of
28 MAX-DOAS with increasing altitudes, and (iii) profiles with box-like shapes, which are not well
29 retrieved with the exponential a priori used.

30



1 3.1.2 Comparison of MAX-DOAS AOD with sun photometer AOD

2 The retrieved BOREAS AOD using UV (360 nm) and visible (477 nm) BOKU MAX-DOAS
3 measurements taken at an azimuth angle of 74° is evaluated against the AOD (average of
4 AERONET AOD at 340 and 380 nm for the UV as well as average of AERONET AOD at 440 and
5 500 nm for the visible channel) obtained from co-located sun photometer observations (see Fig. 4).
6 As already found for the comparison of AE profiles, the best agreement between the two
7 independent AOD measurements is found in fall ($R = 0.95$ and $R = 0.94$ for the UV and visible
8 channel, respectively). While BOREAS generally underestimates AOD in the UV channel, AOD
9 obtained in the visible channel is slightly overestimated during fall and spring. Lower BOREAS
10 AODs are expected because of the limited sensitivity of MAX-DOAS profiling for higher altitudes,
11 e.g. above 4 km (Bösch et al., 2018), whereas AERONET AODs better represent elevated aerosol
12 in the free troposphere and stratosphere. Although the relative contribution of aerosols above 4 km,
13 e.g. in the free troposphere and/or stratosphere, is expected to be rather low over the urban
14 environment of Vienna, Saharan dust aerosols which are released into the atmosphere and can be
15 transported over thousands of kilometers can not be ruled out, in particular during the spring season
16 as indicated by on-line aerosol measurements taken at the Sonnblick Observatory (3106 m a.s.l.)
17 in the Austrian Central Alps (e.g. Greilinger et al., 2019). One explanation for the overestimations
18 noticed in the visible channel of the BOREAS retrievals could be linked to spatial variations of
19 AOD over the urban environment of Vienna, which will be discussed later in section 3.2. As a
20 consequence of different viewing geometries (e.g. 74° azimuthal pointing with the MAX-DOAS
21 vs. direct sun observations with the sun photometer), the two measurements do not always sample
22 the same air masses.

23 While near-surface AE is generally lower in spring than in winter (see Sect. 3.1.1), the opposite
24 appears for AOD with the highest values found in spring, perhaps due to dust events mentioned
25 above.

26

27 3.1.3 Comparison of MAX-DOAS near-surface AE with in situ surface PM10



1 In addition to the evaluation of BOREAS near-surface AE against ceilometer observations (see
2 Sect. 3.1.1), AE is compared against surface in situ measurements of particulate matter. Near-
3 surface AE can be extracted from both ceilometer AE profiles and MAX-DOAS/BOREAS
4 retrievals. The evaluation is performed through comparison with surface PM10 concentrations
5 obtained from the air quality monitoring station “Gerichtsgasse (Floridsdorf)”, which is about 5.5
6 and 3.25 kilometers away from the BOKU MAX-DOAS and ceilometer, respectively (see Fig. 1).
7 It should be noted that AE and PM10 are two different physical quantities and thus, a perfect
8 correlation is not expected. In agreement with the previous findings, the BOREAS AE retrievals in
9 the UV and visible channels are qualitatively most consistent with ambient surface PM10
10 concentrations during the fall, winter, and spring seasons (see Fig. 5 and Fig. 6). For the near-
11 surface AE retrieved in the UV channel, the strongest correlation with $R = 0.78$ is found for the fall
12 season. The slopes and intercepts of the linear regression characterizing the BOREAS AE and the
13 PM10 datasets are in very good agreement with those obtained from the linear regression between
14 the ceilometer AE and surface PM10 concentrations in that season of the year, but also in winter
15 and spring. This result highlights the strong performance of BOREAS, in particular for the lowest
16 100 m. It should be noted that BOKU and ZAMG sites are located in suburban areas, whereas the
17 location of the in situ station “Gerichtsgasse” is characterized as urban (Spangl, 2019). This could
18 explain the larger scatter observed during winter, which might be the result of a combination of
19 spatial differences in emission strength, different measuring heights, and rather stable
20 meteorological conditions, thus favoring less mixing of aerosols.

21

22 **3.2 Spatial variability of AOD and near-surface AE**

23 To better understand the spatial variabilities of AOD and near-surface AE and the origin of aerosols
24 over the urban environment of Vienna, combined MAX-DOAS aerosol and NO₂ profiling products
25 were used. Towards this direction, the MAX DOAS UV data for the five (BOKU) and six (Arsenal)
26 azimuthal angles (see Fig. 1) were analyzed in more detail. Because of the rather weaker
27 performance of BOREAS during summer, the results of the following analysis are presented for
28 the fall, winter, and spring seasons. In order to make the MAX-DOAS measurements of all viewing
29 directions comparable, the retrieved AOD and near-surface AE together with the NO₂ retrieval



1 products of tropospheric NO₂ vertical column density (VCD NO₂) and near-surface NO₂
2 concentrations, are interpolated to half-hour intervals. In a second step, only those time intervals
3 with available AOD, near-surface AE, VCD NO₂, and near-surface NO₂ observations at all eleven
4 azimuth angles are considered. Consequently, half-hour intervals with missing observations for at
5 least one azimuth angle are discarded from the data sets. Inevitably, this filtering procedure further
6 reduces the number of aerosol profiles obtained during cloud-free conditions ($N = 52$ in fall, $N =$
7 24 in winter, and $N = 30$ in spring). After removing half-hour intervals with missing observations,
8 the remaining data points are averaged per azimuth angle and per season, excluding summer as
9 mentioned before.

10 The relationship between the spatial variability of averaged AODs and averaged VCD NO₂ is
11 presented in Fig. 7. The results reveal that higher AOD values (e.g. the vertically integrated AE)
12 are detected by the Arsenal MAX-DOAS, whereas higher VCD NO₂ (e.g. the vertically integrated
13 NO₂ concentration) by the BOKU MAX-DOAS. The reason for the lower VCD NO₂ values
14 observed by the Arsenal MAX-DOAS could be that the instrument is installed on a tower platform
15 at 131 m above ground. Thus, NO₂ in the lowest layers close to the surface is not captured by the
16 instrument. Higher AOD amounts at the Arsenal site could be related to industrial emission sources
17 nearby. The highest amounts of both AOD and VCD NO₂, which includes observations from only
18 a couple of cloud-free days, are detected by both instruments during fall. A closer look at the
19 averaged BOKU MAX-DOAS retrieval results reveals that the ratio of the maximum AOD (74°)
20 over the minimum AOD (144°) was 1.07 (fall), 1.13 (winter), and 1.08 (spring). For the VCD NO₂,
21 the opposite trend is observed with the highest values towards the urban core and the lowest in the
22 suburban areas in the north-east. Greater irregularities from this pattern, but still significant spatial
23 differences are found for the Arsenal MAX-DOAS with the averaged AOD maximum (348°) in
24 spring, being also ~10% higher than the minimum (324°).

25 Similarly, the spatial patterns of averaged near-surface AE, in relation to averaged near-surface
26 NO₂ concentrations, are illustrated in Fig. 8. Overall, near-surface AE increases with increasing
27 NO₂ concentrations, suggesting that both aerosols and nitrogen oxides (NO_x) are released from
28 anthropogenic emission sources. The highest values for both near-surface AE and NO₂ are found
29 in winter, followed by fall and spring. Interestingly, the highest winter amounts of both near-
30 surface AE and NO₂ are observed when the BOKU MAX-DOAS instrument is measuring at an



1 azimuth angle of 88° . Along the respective light path of this viewing direction, heavy-traffic roads
2 and a heat-generating power-station (waste incineration plant in Spittelau, 48.2344° N, 16.3594°
3 E) can be found. In contrast, AE and NO_2 near-surface amounts are second-lowest at this viewing
4 direction during fall and spring, which could be interpreted as an indication of a significant
5 contribution of the heat-generating power-station to local air pollution in winter. As expected,
6 higher spatial differences are found for the near-surface aerosol and NO_2 profiling products than
7 for column-integrated retrieval results. While average BOKU MAX-DOAS retrieval results reveal
8 that maximum near-surface AE (144°) is higher than minimum near-surface AE (74°) by a factor
9 of 1.32 in spring, the largest relative difference between maximum (324°) and minimum (10°)
10 averages of 25% is observed for the Arsenal MAX-DOAS retrievals in winter.

11

12 **4 Summary and outlook**

13 In this study, an evaluation of BOREAS aerosol profiling products is presented by comparing AE
14 profiles, AOD, and near-surface AE retrieved from UV and visible MAX-DOAS measurements
15 with data from co-located ceilometer, sun photometer, and in situ instruments. It is the first time
16 that AE profiles are reported for different seasons and daytimes over the urban environment of
17 Vienna.

18 Both the location and viewing direction of the BOKU MAX-DOAS are arranged in a way to cover
19 as much as possible of the vertical extent of the measurements taken by the ceilometer, resulting
20 in an overlap of an altitude up to 4 km. The rather short distance of 2.25 km between the BOKU
21 MAX-DOAS and ceilometer further reduces effects that could arise from spatial variations. In
22 addition to the evaluation of the vertical AE profiles, measurements of co-located sun photometer
23 (a few meters away) and in situ instruments are obtained to assess the quality of vertically-
24 integrated and near-surface BOREAS retrieval results.

25 In contrast to the recent BOREAS-based profile studies (Bösch et al., 2018; Gratsea et al., 2020;
26 Tirpitz et al., 2020), this study takes into account measured atmospheric profiles of pressure and
27 temperature taken at a co-located site of the Austrian official weather service (e.g. the same site
28 where the ceilometer is operated). To systematically evaluate the retrieved BOREAS aerosol



1 profiling products in Vienna, MAX-DOAS measurements from more than a hundred cloud-free
2 days covering all seasons of the 2017-2019 period are considered.

3 The results of this study show that the retrieved BOREAS AE profiles from the BOKU MAX-
4 DOAS measurements are consistent with AE profiles from the co-located ceilometer. The highest
5 correlation coefficients of 0.91-0.99 (UV) and 0.85-0.98 (visible) are found for the fall, winter, and
6 spring seasons. The largest discrepancies between the two independent measurements arise during
7 summer, most probably as a result of elevated mixing-heights leading to pronounced vertical
8 mixing of air masses. The good performance of BOREAS is underlined by the agreement found
9 when AOD and near-surface AE are compared with AERONET AOD and in situ PM10
10 measurements, again with the exception of summer. A summary of correlation coefficients
11 obtained in this study is given in Table 2.

12 After resampling BOREAS aerosol profiling products, the spatial variability of vertically-
13 integrated and near-surface aerosol amounts was investigated. While relative differences of the
14 mean AOD retrieved from MAX-DOAS measurements taken at different azimuth angles are on
15 the order of 7-13%, larger relative differences of up to 32% between averaged values obtained for
16 the different viewing directions are found for near-surface AE. The high correlation of the near-
17 surface AE and near-surface NO₂ suggests that the aerosol layer close to the ground is mainly of
18 anthropogenic origin. However, cases of high AOD are sometimes also found at low NO₂ VCDs,
19 most probably as a consequence of trans-boundary pollution and/or dust events that temporally
20 affect air masses above the urban environment of Vienna.

21 In conclusion, good agreement between MAX-DOAS aerosol profiling products and data from co-
22 located instruments is found, highlighting the strong performance of BOREAS for the retrieval of
23 tropospheric vertical aerosol profiles covering the range between the instrument's altitude up to 4
24 km as well as its capability to detect spatial variations of aerosol amounts over urban environments.

25

26 **Data availability.** Data can be requested from the corresponding author
27 (stefan.schreier@boku.ac.at).

28



1 **Author contributions.** SFS, TB, and AR formulated the overarching goals of this study. TB
2 performed calculations with the MAX-DOAS profile retrieval algorithmn BOREAS. SFS applied
3 the method to convert ceilometer backscatter profiles into aerosol extinction profiles. PW applied
4 a RTM to simulate global radiation and MR developed the procedure to select cloud-free days. SFS
5 performed the analyses and prepared the manuscript. SFS and AR are responsible for the
6 continuous operation of the BOKU MAX-DOAS instrument. SFS, AR, KL, and MV are
7 responsible for the continuous operation of the Arsenal MAX-DOAS instrument. PW as the
8 principle investigator of the AERONET Vienna_BOKU site provided the sun photometer
9 measurements. CL is responsible for the continuous operation of the ZAMG ceilometer and
10 provided both range-corrected backscatter and mixing-height data. All authors contributed to the
11 writing of this manuscript.

12

13 **Competing interests.** Andreas Richter is a member of the editorial board of the journal.

14

15 **Acknowledgements.** This study was funded by the Austrian Science Fund (FWF): I 2296-N29,
16 the German Science Foundation (DFG): Ri 1800/6-1, and A1 Telekom Austria. Special thanks go
17 to Werner Sagmeister and Helmut Kropf from A1 Telekom for their organizational and technical
18 support. Our thanks go to the University of Wyoming for making available the atmospheric
19 sounding data. We would like to thank “Amt der Wiener Landesregierung” and
20 “Umweltbundesamt” for making the air quality (e.g. PM10) data freely available. Many thanks go
21 to the (extended) VINDOBONA team for helping to establish a MAX-DOAS measurement
22 network in Vienna. Finally, we would like to thank the BOKU-Met weather station team for
23 helping to maintain meteorological instruments and making freely available its data.

24

25 **References**

26 Ansmann, A., Tesche, M., Seifert, P., Groß, S., Freudenthaler, V., Apituley, A., Wilson, K. M.,
27 Serikov, I., Linné, H., Heinold, B., Hiebsch, A., Schnell, F., Schmidt, J., Mattis, I., Wandinger, U.,



- 1 and Wiegner, M.: Ash and fine mode particle mass profiles from EARLINET/AERONET
2 observations over central Europe after the eruptions of the Eyjafjallajökull volcano in 2010, *J.*
3 *Geophys.Res.*, 116, D16S02, doi:10.1029/2003JD004047, 2011.
- 4 Baumann-Stanzer, K., Greilinger, M., Kasper-Giebl, A., Flandorfer, C., Hieden, A., Lotteraner, C.,
5 Ortner, M., Vergeiner, J., Schauer, G., Piringer, M.: Evaluation of WRF-Chem Model Forecasts of
6 a Prolonged Sahara Dust Episode over the Eastern Alps. *Aerosol and Air Quality Research*19,
7 1226-1240, DOI: 10.4209/aaqr.2018.03.0116, 2019.
- 8 Behrens, L. K., Hilboll, A., Richter, A., Peters, E., Alvarado, L. M. A., Kalisz Hedegaard, A. B.,
9 Wittrock, F., Burrows, J. P., and Vrekoussis, M.: Detection of outflow of formaldehyde and glyoxal
10 from the African continent to the Atlantic Ocean with a MAX-DOAS instrument, *Atmos. Chem.*
11 *Phys.*, 19, 10257–10278, <https://doi.org/10.5194/acp-19-10257-2019>, 2019.
- 12 Beirle, S., Dörner, S., Donner, S., Remmers, J., Wang, Y., and Wagner, T.: The Mainz profile
13 algorithm (MAPA), *Atmos. Meas. Tech.*, 12, 1785–1806, [https://doi.org/10.5194/amt-12-1785-](https://doi.org/10.5194/amt-12-1785-2019)
14 2019, 2019.
- 15 Bösch, T., Rozanov, V., Richter, A., Peters, E., Rozanov, A., Wittrock, F., Merlaud, A., Lampel,
16 J., Schmitt, S., de Haij, M., Berkhout, S., Henzing, B., Apituley, A., den Hoed, M., Vonk, J.,
17 Tiefengraber, M., Müller, M., and Burrows, J. P.: BOREAS – a new MAX-DOAS profile retrieval
18 algorithm for aerosols and trace gases, *Atmos. Meas. Tech.*, 11, 6833-6859,
19 <https://doi.org/10.5194/amt-11-6833-2018>, 2018.
- 20 Chan, K. L., Wiegner, M., Wenig, M., and Pöhler, D.: Observations of tropospheric aerosols and
21 NO₂ in Hong Kong over 5 years using ground based MAX-DOAS, *Sci. Total Environ.*, 619, 1545–
22 1556, <https://doi.org/10.1016/j.scitotenv.2017.10.153>, 2017.
- 23 Clémer, K., Van Roozendaal, M., Fayt, C., Hendrick, F., Hermans, C., Pinardi, G., Spurr, R., Wang,
24 P., and De Mazière, M.: Multiple wavelength retrieval of tropospheric aerosol optical properties
25 from MAXDOAS measurements in Beijing, *Atmos. Meas. Tech.*, 3, 863–878,
26 <https://doi.org/10.5194/amt-3-863-2010>, 2010.



- 1 Donner, S., Kuhn, J., Van Roozendael, M., Bais, A., Beirle, S., Bösch, T., Bognar, K., Bruchkouski,
2 I., Chan, K. L., Dörner, S., Drosoglou, T., Fayt, C., Frieß, U., Hendrick, F., Hermans, C., Jin, J.,
3 Li, A., Ma, J., Peters, E., Pinardi, G., Richter, A., Schreier, S. F., Seyler, A., Strong, K., Tirpitz, J.-
4 L., Wang, Y., Xie, P., Xu, J., Zhao, X., and Wagner, T.: Evaluating different methods for elevation
5 calibration of MAX-DOAS (Multi AXis Differential Optical Absorption Spectroscopy)
6 instruments during the CINDI-2 campaign, *Atmos. Meas. Tech.*, 13, 685–712,
7 <https://doi.org/10.5194/amt-13-685-2020>, 2020.
- 8 Friedrich, M. M., Rivera, C., Stremme, W., Ojeda, Z., Arellano, J., Bezanilla, A., García-Reynoso,
9 J. A., and Grutter, M.: NO₂ vertical profiles and column densities from MAX-DOAS
10 measurements in Mexico City, *Atmos. Meas. Tech.*, 12, 2545–2565, [https://doi.org/10.5194/amt-](https://doi.org/10.5194/amt-12-2545-2019)
11 [12-2545-2019](https://doi.org/10.5194/amt-12-2545-2019), 2019.
- 12 Frieß, U., Monks, P. S., Remedios, J. J., Rozanov, A., Sinreich, R., Wagner, T., and Platt, U.:
13 MAX-DOAS O₄ measurements: A new technique to derive information on atmospheric aerosols
14 (II), *Modelling studies*, *J. Geophys. Res.*, 111, D14203, [doi:10.1029/2005JD006618](https://doi.org/10.1029/2005JD006618), 2006.
- 15 Frieß, U., Klein Baltink, H., Beirle, S., Clémer, K., Hendrick, F., Henzing, B., Irie, H., de Leeuw,
16 G., Li, A., Moerman, M. M., van Roozendael, M., Shaiganfar, R., Wagner, T., Wang, Y., Xie, P.,
17 Yilmaz, S., and Zieger, P.: Intercomparison of aerosol extinction profiles retrieved from MAX-
18 DOAS measurements, *Atmos. Meas. Tech.*, 9, 3205–3222, [https://doi.org/10.5194/amt-9-3205-](https://doi.org/10.5194/amt-9-3205-2016)
19 [2016](https://doi.org/10.5194/amt-9-3205-2016), 2016.
- 20 Frieß, U., Beirle, S., Alvarado Bonilla, L., Bösch, T., Friedrich, M. M., Hendrick, F., PETERS, A.,
21 Richter, A., van Roozendael, M., Rozanov, V. V., Spinei, E., Tirpitz, J.-L., Vlemmix, T., Wagner,
22 T., and Wang, Y.: Intercomparison of MAX-DOAS vertical profile retrieval algorithms: studies
23 using synthetic data, *Atmos. Meas. Tech.*, 12, 2155–2181, [https://doi.org/10.5194/amt-12-2155-](https://doi.org/10.5194/amt-12-2155-2019)
24 [2019](https://doi.org/10.5194/amt-12-2155-2019), 2019.
- 25 Gratsea, M., Bösch, T., Kokkalis, P., Richter, A., Vrekoussis, M., Kazadzis, S., Tsekeri, A.,
26 Papayannis, A., Mylonaki, M., Amiridis, V., Mihalopoulos, N., and Gerasopoulos, E.: Retrieval
27 and evaluation of tropospheric aerosol extinction profiles using MAX-DOAS measurements over



- 1 Athens, Greece, *Atmos. Meas. Tech. Discuss.*, <https://doi.org/10.5194/amt-2020-100>, in review,
2 2020.
- 3 Greilinger, M., Zbiral, J., and Kasper-Giebl, A: Desert Dust Contribution to PM10 Loads in Styria
4 (Southern Austria) and Impact on Exceedance of Limit Values from 2013–2018, *Appl. Sci.* 9(11),
5 2265; <https://doi.org/10.3390/app9112265>, 2019.
- 6 Holben, B. N., Eck, T. F., Slutsker, I., Tanré, D., Buis, J. P., Setzer, A., Vermote, E., Reagan, J.
7 A., Kaufman, Y. J., Nakajima, T., Lavenu, F., Jankowiak, I., and Smirnov, A.: AERONET – A
8 Federated Instrument Network and Data Archive for Aerosol Characterization, *Remote Sens.*
9 *Environ.*, 66, 1–16, 1998.
- 10 IPCC: Summary for Policymakers, in: *Climate Change 2013: The Physical Science Basis*,
11 *Contribution of Working Group I to the Fifth Assessment Report of the Intergovernmental Panel*
12 *on Climate Change*, edited by: Stocker, T. F., Qin, D., Plattner, G.-K., Tignor, M., Allen, S. K.,
13 Boschung, J., Nauels, A., Xia, Y., Bex, V., and Midgley, P. M., Cambridge University Press,
14 Cambridge, UK, New York, NY, USA, 2013.
- 15 Kanakidou, M., Myriokefalitakis, S., and Tsigaridis, K.: Aerosols in atmospheric chemistry and
16 biogeochemical cycles of nutrients, *Environ. Res. Lett.*, 13, 063004, [https://doi.org/10.1088/1748-](https://doi.org/10.1088/1748-9326/aabddb)
17 [9326/aabddb](https://doi.org/10.1088/1748-9326/aabddb), 2018.
- 18 Lelieveld, J., Evans, J. S., Fnais, M., Giannadaki, D., and Pozzer, A.: The contribution of outdoor
19 air pollution sources to pre-mature mortality on a global scale, *Nature*, 525, 367–371,
20 [doi:10.1038/nature15371](https://doi.org/10.1038/nature15371), 2015.
- 21 Lotteraner, C. and Piringer, M.: Mixing-Height Time Series from Operational Ceilometer Aerosol-
22 Layer Heights, *Bound.-Lay. Meteorol.*, 161, 265–287, [https://doi.org/10.1007/s10546-016-0169-](https://doi.org/10.1007/s10546-016-0169-2)
23 [2](https://doi.org/10.1007/s10546-016-0169-2), 2016.
- 24 Ma, J. Z., Beirle, S., Jin, J. L., Shaiganfar, R., Yan, P., and Wagner, T.: Tropospheric NO₂ vertical
25 column densities over Beijing: results of the first three years of ground-based MAX-DOAS
26 measurements (2008–2011) and satellite validation, *Atmos. Chem. Phys.*, 13, 1547–1567,
27 <https://doi.org/10.5194/acp-13-1547-2013>, 2013.



- 1 Madonna, F., Rosoldi, M., Lolli, S., Amato, F., Vande Hey, J., Dhillon, R., Zheng, Y., Brettle, M.,
2 and Pappalardo, G.: Intercomparison of aerosol measurements performed with multi-wavelength
3 Raman lidars, automatic lidars and ceilometers in the framework of INTERACT-II campaign,
4 *Atmos. Meas. Tech.*, 11, 2459–2475, <https://doi.org/10.5194/amt-11-2459-2018>, 2018.
- 5 Mayer, B. and Kylling, A.: Technical note: The libRadtran software package for radiative transfer
6 calculations - description and examples of use, *Atmos. Chem. Phys.*, 5, 1855–1877,
7 <https://doi.org/10.5194/acp-5-1855-2005>, 2005.
- 8 Peters, E., Wittrock, F., Großmann, K., Friß, U., Richter, A., and Burrows, J. P.: Formaldehyde
9 and nitrogen dioxide over the remote western Pacific Ocean: SCIAMACHY and GOME-2
10 validation using ship-based MAX-DOAS observations, *Atmos. Chem. Phys.*, 12, 11179–11197,
11 <https://doi.org/10.5194/acp-12-11179-2012>, 2012.
- 12 Peters, E.: Improved MAX-DOAS measurements and retrievals focused on the marine boundary
13 layer, Dissertation, University of Bremen, Bremen, 2013.
- 14 Rodgers, C. D.: Inverse Methods for Atmospheric Sounding: Theory and Practice, in: Series on
15 atmospheric oceanic and planetary physics, Vol. 2, World Scientific, Singapore, reprinted edn.,
16 oCLC: 254137862, 2004.
- 17 Roscoe, H. K., Van Roozendaal, M., Fayt, C., du Piesanie, A., Abuhassan, N., Adams, C., Akrami,
18 M., Cede, A., Chong, J., Clémer, K., Friess, U., Gil Ojeda, M., Goutail, F., Graves, R., Griesfeller,
19 A., Grossmann, K., Hemerijckx, G., Hendrick, F., Herman, J., Hermans, C., Irie, H., Johnston, P.
20 V., Kanaya, Y., Kreher, K., Leigh, R., Merlaud, A., Mount, G. H., Navarro, M., Oetjen, H.,
21 Pazmino, A., Perez-Camacho, M., Peters, E., Pinardi, G., Puentedura, O., Richter, A., Schönhardt,
22 A., Shaiganfar, R., Spinei, E., Strong, K., Takashima, H., Vlemmix, T., Vrekoussis, M., Wagner,
23 T., Wittrock, F., Yela, M., Yilmaz, S., Boersma, F., Hains, J., Kroon, M., Piters, A., and Kim, Y.
24 J.: Intercomparison of slant column measurements of NO₂ and O₄ by MAX-DOAS and zenith-sky
25 UV and visible spectrometers, *Atmos. Meas. Tech.*, 3, 1629–1646, [https://doi.org/10.5194/amt-3-](https://doi.org/10.5194/amt-3-1629-2010)
26 1629-2010, 2010.



- 1 Rozanov, V., Rozanov, A., Kokhanovsky, A., and Burrows, J.: Ra-diative transfer through
2 terrestrial atmosphere and ocean: soft-ware package SCIATRAN, *J. Quant. Spectrosc. Ra.*, 133,
3 13–71, doi:10.1016/j.jqsrt.2013.07.004, 2014.
- 4 Schreier, S. F., Peters, E., Richter, A., Lampel, J., Wittrock, F., and Burrows, J. P.: Ship-based
5 MAX-DOAS measurements of tropospheric NO₂ and SO₂ in the South China and Sulu Sea,
6 *Atmos. Environ.*, 102, 331–343, <https://doi.org/10.1016/j.atmosenv.2014.12.015>, 2015.
- 7 Schreier, S. F., Richter, A., Peters, E., Ostendorf, M., Schmalwieser, A. W., Weihs, P., and
8 Burrows, J. P.: Dual ground-based MAX-DOAS observations in Vienna, Austria: Evaluation of
9 horizontal and temporal NO₂, HCHO, and CHOCHO distributions and comparison with
10 independent data sets, *Atmospheric Environment: X*, 5, 100059,
11 <https://doi.org/https://doi.org/10.1016/j.aeaoa.2019.100059>, 2020.
- 12 Seinfeld, J. H. and Pandis, S. N.: *Atmospheric Chemistry and Physics: From Air Pollution to*
13 *Global Change*, second ed., J. Wiley and Sons, New York, USA, 2006.
- 14 Spangl, W.: *Luftgütemessstellen in Österreich*, REPORT REP 0674, Umweltbundesamt GmbH,
15 Wien, 2019.
- 16 Stamnes, K., Tsay, S., Wiscombe, W., and Jayaweera, K.: A numerically stable algorithm for
17 discrete-ordinate-method radiative transfer in multiple scattering and emitting layered media,
18 *Appl. Opt.*, 27, 2502–2509, <https://doi.org/10.1364/AO.27.002502>, 1988.
- 19 Tirpitz, J.-L., Frieß, U., Hendrick, F., Alberti, C., Allaart, M., Apituley, A., Bais, A., Beirle, S.,
20 Berkhout, S., Bognar, K., Bösch, T., Bruchkouski, I., Cede, A., Chan, K. L., den Hoed, M., Donner,
21 S., Drosoglou, T., Fayt, C., Friedrich, M. M., Frumau, A., Gast, L., Gielen, C., Gomez-Martín, L.,
22 Hao, N., Hensen, A., Henzing, B., Hermans, C., Jin, J., Kreher, K., Kuhn, J., Lampel, J., Li, A.,
23 Liu, C., Liu, H., Ma, J., Merlaud, A., Peters, E., Pinardi, G., Piters, A., Platt, U., Puentedura, O.,
24 Richter, A., Schmitt, S., Spinei, E., Stein Zweers, D., Strong, K., Swart, D., Tack, F., Tiefengraber,
25 M., van der Hoff, R., van Roozendael, M., Vlemmix, T., Vonk, J., Wagner, T., Wang, Y., Wang,
26 Z., Wenig, M., Wiegner, M., Wittrock, F., Xie, P., Xing, C., Xu, J., Yela, M., Zhang, C., and Zhao,
27 X.: Intercomparison of MAX-DOAS vertical profile retrieval algorithms: studies on field data from



- 1 the CINDI-2 campaign, *Atmos. Meas. Tech. Discuss.*, <https://doi.org/10.5194/amt-2019-456>, in
2 review, 2020.
- 3 Vlemmix, T., Hendrick, F., Pinardi, G., De Smedt, I., Fayt, C., Hermans, C., Pitters, A., Wang, P.,
4 Levelt, P., and Van Roozendael, M.: MAX-DOAS observations of aerosols, formaldehyde and
5 nitrogen dioxide in the Beijing area: comparison of two profile retrieval approaches, *Atmos. Meas.*
6 *Tech.*, 8, 941–963, <https://doi.org/10.5194/amt-8-941-2015>, 2015.
- 7 Wagner, P. and Schäfer, K.: Influence of mixing layer height on air pollutant concentrations in an
8 urban street canyon, *Urban Climate*, <https://doi.org/10.1016/j.uclim.2015.11.001>, 2015.
- 9 Wagner, T., Dix, B., von Friedeburg, C., Frieß, U., Sanghavi, S., Sinreich, R., and Platt, U.: MAX-
10 DOAS O₄ measurements: A new technique to derive information on atmospheric aerosols –
11 Principles and information content, *J. Geophys. Res.*, 109, D22205,
12 <https://doi.org/10.1029/2004JD004904>, 2004.
- 13 Wagner, T., Beirle, S., Benavent, N., Bösch, T., Chan, K. L., Donner, S., Dörner, S., Fayt, C., Frieß,
14 U., García-Nieto, D., Gielen, C., González-Bartolome, D., Gomez, L., Hendrick, F., Henzing, B.,
15 Jin, J. L., Lampel, J., Ma, J., Mies, K., Navarro, M., Peters, E., Pinardi, G., Puentedura, O., Puçite,
16 J., Remmers, J., Richter, A., Saiz-Lopez, A., Shaiganfar, R., Sihler, H., Van Roozendael, M.,
17 Wang, Y., and Yela, M.: Is a scaling factor required to obtain closure between measured and
18 modelled atmospheric O₄ absorptions? An assessment of uncertainties of measurements and
19 radiative transfer simulations for 2 selected days during the MAD-CAT campaign, *Atmos. Meas.*
20 *Tech.*, 12, 2745–2817, <https://doi.org/10.5194/amt-12-2745-2019>, 2019.
- 21 Wang, Y., Li, A., Xie, P.-H., Chen, H., Xu, J., Wu, F.-C., Liu, J.-G., and Liu, W.-Q.: Retrieving
22 vertical profile of aerosol extinction by multi-axis differential optical absorption spectroscopy,
23 *Acta Physica Sinica*, 62, 180705, <https://doi.org/10.7498/aps.62.180705>, 2013.
- 24 Wang, Y., Beirle, S., Hendrick, F., Hilboll, A., Jin, J., Kyuberis, A. A., Lampel, J., Li, A., Luo, Y.,
25 Lodi, L., Ma, J., Navarro, M., Ortega, I., Peters, E., Polyansky, O. L., Remmers, J., Richter, A.,
26 Puentedura, O., Van Roozendael, M., Seyler, A., Tennyson, J., Volkamer, R., Xie, P., Zobov, N.
27 F., and Wagner, T.: MAX-DOAS measurements of HONO slant column densities during the



1 MAD-CAT campaign: inter-comparison, sensitivity studies on spectral analysis settings, and error
2 budget, *Atmos. Meas. Tech.*, 10, 3719–3742, <https://doi.org/10.5194/amt-10-3719-2017>, 2017.

3 Wittrock, F.: The Retrieval of Oxygenated Volatile Organic Compounds by Remote Sensing
4 Techniques, Dissertation, University of Bremen, Bremen, 2006.

5 Yilmaz, S.: Retrieval of atmospheric aerosol and trace gas vertical profiles using multi-axis
6 differential optical absorption spectroscopy, Ph.D. thesis, Heidelberg, Univ., Diss., 2012, available
7 at: <http://archiv.ub.uni-heidelberg.de/volltextserver/volltexte/2012/13128> (last access: January
8 2021), 2012.

9

10

11

12

13

14

15

16

17

18

19

20

21

22



1 Table 1. Locations, data products, and characteristics of the instruments used in this study.

Instrument	Location	Manufacturer	Data products	Temporal resolution	Start of measurements	Reference
MAX-DOAS (BOKU)	48.2379°N 16.3317°E 267 m a.s.l.	custom-made	AE profiles AOD near-surface AE	35-70 min ^a	May 2017	Schreier et al. (2020)
MAX-DOAS (Arsenal)	48.1818°N 16.3908°E 333 m a.s.l.	custom-made	AE profiles AOD near-surface AE	35-70 min ^a	August 2018	Behrens et al. (2019)
Ceilometer	48.2483°N 16.3564°E 198 m a.s.l.	VAISALA	AE profiles	~ 30 s	July 2012	Lotteraner & Piringer (2016)
Sun photometer	48.2379°N 16.3317°E 267 m a.s.l.	CIMEL	AOD	~ 3min	May 2016	Holben et al. (1998)
In situ monitor	48.2611°N 16.3969°E 164 m a.s.l.	GRIMM	surface PM10	30 min	January 2017	Spangl (2019)
Star pyranometer	48.2379°N 16.3316°E 266 m a.s.l.	SCHENK	Global radiation	10 min	March 2005	-

2

3 ^a temporal resolution refers to the time span between recurring elevation sequences at one specific azimuth angle

4

5

6

7

8

9

10

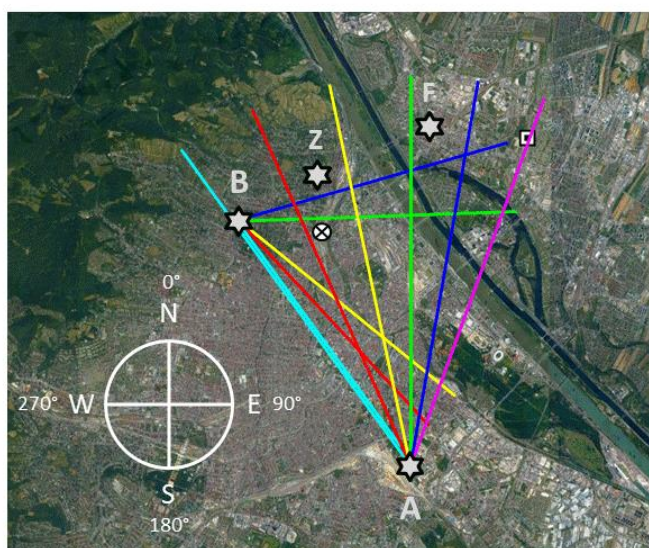
11



1 Table 2. Summary of correlations obtained in this study.

<i>R</i>	vertical AE profiles		near-surface AE				AOD	
	MAX-DOAS vs. ceilometer		MAX-DOAS vs. ceilometer		MAX-DOAS vs. in situ		BOREAS vs. AERONET	
	UV	visible	UV	visible	UV	visible	UV	visible
Fall	0.915-0.973	0.840-0.975	0.917	0.901	0.782	0.814	0.953	0.939
Winter	0.943-0.989	0.879-0.980	0.916	0.849	0.765	0.739	0.903	0.874
Spring	0.905-0.944	0.891-0.975	0.723	0.823	0.777	0.825	0.799	0.924
Summer	0.769-0.957	0.458-0.955	0.276	0.350	0.286	0.369	0.370	0.505

2
 3
 4
 5
 6
 7
 8
 9
 10
 11
 12
 13
 14
 15
 16
 17

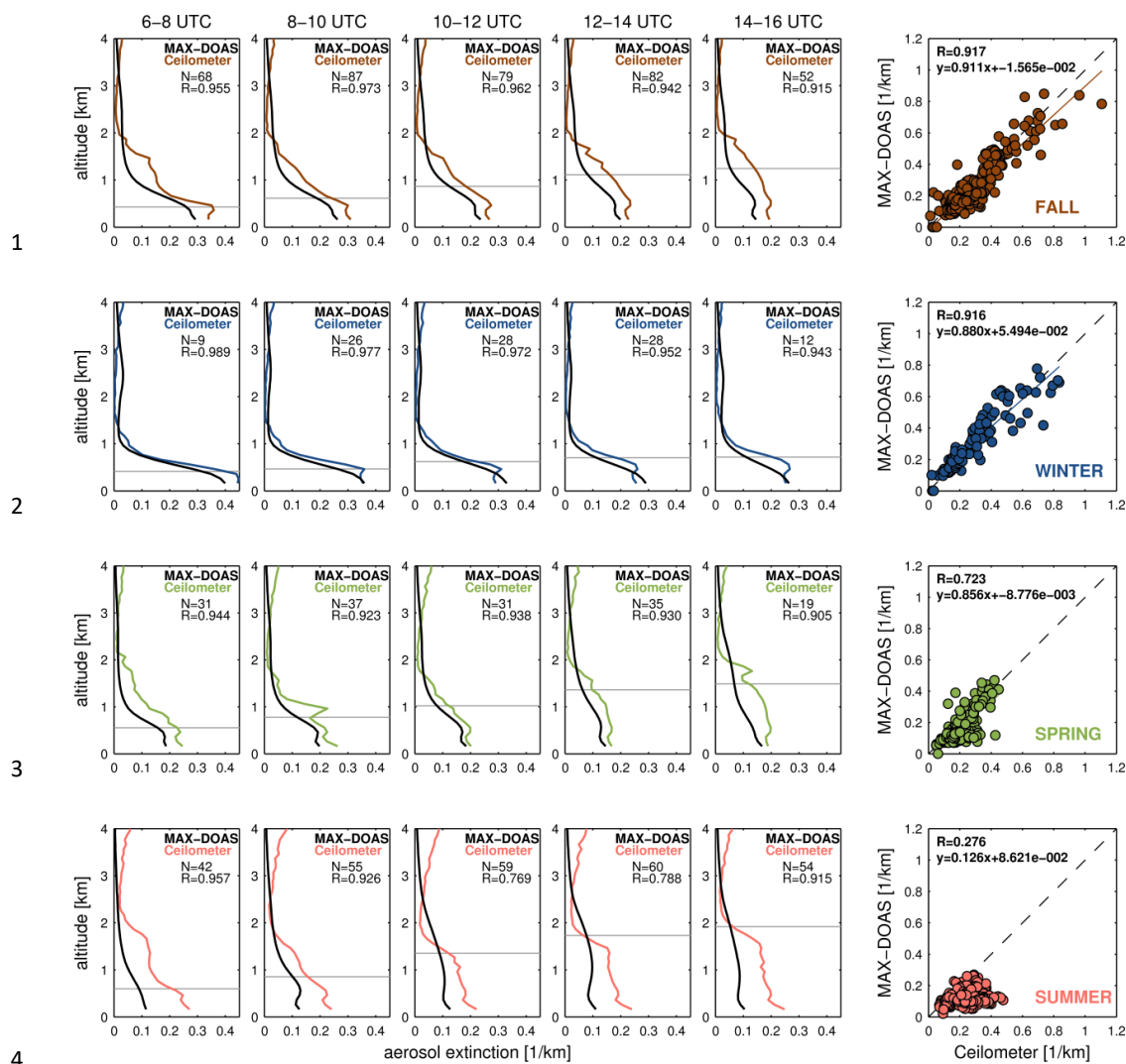


1

2 Figure 1. Geographical location of co-located instruments considered in this study: Arsenal (A)
3 and BOKU (B) MAX-DOAS with their associated azimuthal viewing directions (in clockwise
4 direction): 324° (cyan), 336° (red), 348° (yellow), 0° (green), 10° (blue), and 20° (magenta)
5 (Arsenal MAX-DOAS) as well as 74° (blue), 88° (green), 129° (yellow), 137° (red), and 144°
6 (cyan) (BOKU MAX-DOAS). Ceilometer (Z), sun photometer (B), and in situ (F) instruments are
7 located close to the 74° azimuthal viewing direction of the BOKU MAX-DOAS. The linear
8 distance between the two MAX-DOAS instruments is ~7.5 kilometers. The cross in circle symbol
9 indicates the location of the waste incineration plant. Image © Google Earth.

10

11



5 Figure 2. Averaged vertical AE [1/km] profiles retrieved from BOKU MAX-DOAS (B, see Fig. 1)
 6 at 74° azimuth angle (black solid lines) and ceilometer (Z, see Fig. 1) (color-coded solid lines)
 7 observations (left panels) for selected time periods and the four seasons fall (SON), winter (DJF),
 8 spring (MAM), and summer (JJA). The gray horizontal lines illustrate corresponding averages of
 9 mixing-heights from ceilometer measurements. Scatter plots of MAX-DOAS and ceilometer near-
 10 surface AE for the different seasons are shown in the right panels. Data of cloud-free days as
 11 defined in Sect. 2.2.1 between 1 September 2017 and 31 August 2019 are included. The



1 measurements shown here are representative for the UV channel (MAX-DOAS: 338-370 nm,
2 ceilometer: 360 nm).

3

4

5

6

7

8

9

10

11

12

13

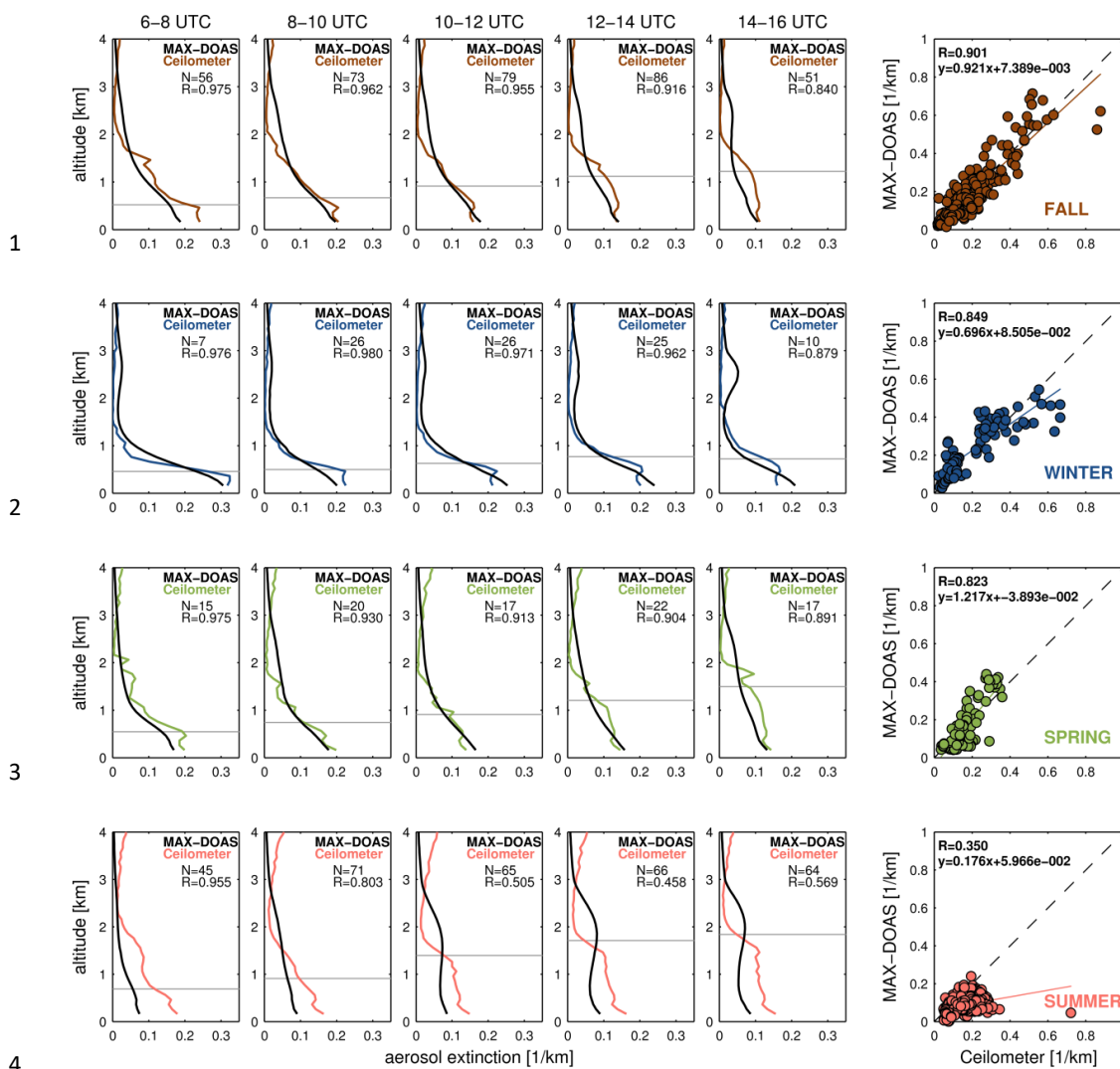
14

15

16

17

18

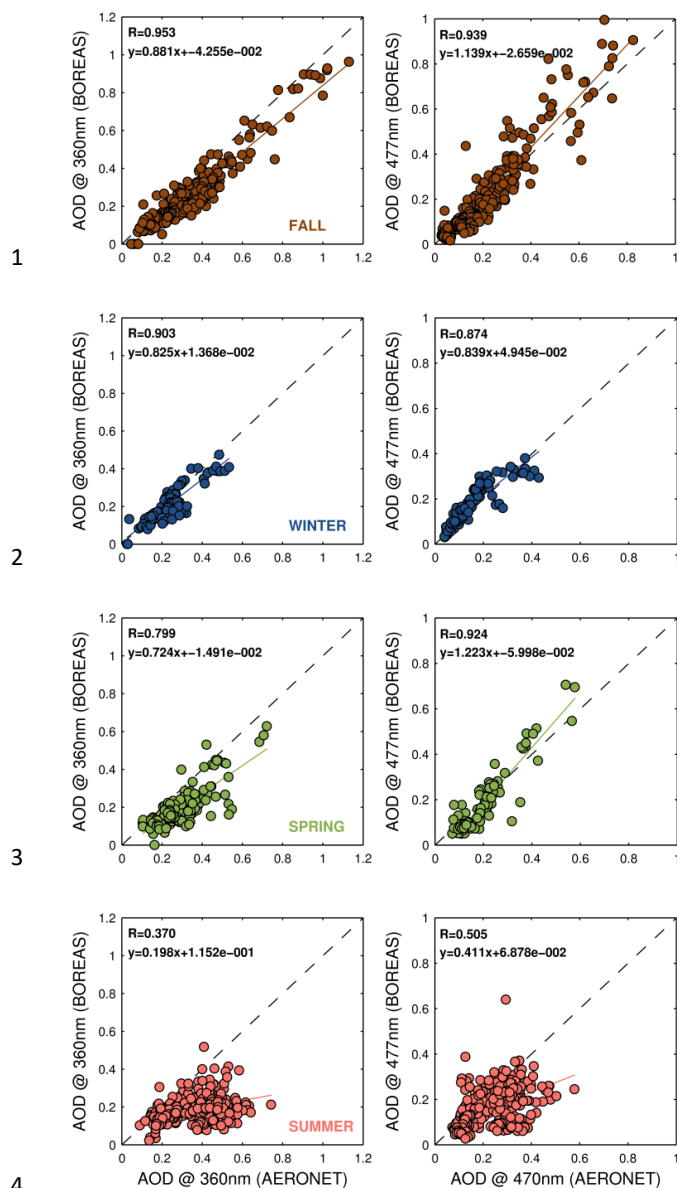


5 Figure 3. Same as Fig. 2, but for the visible channel (MAX-DOAS: 425-490 nm, ceilometer: 470
 6 nm).

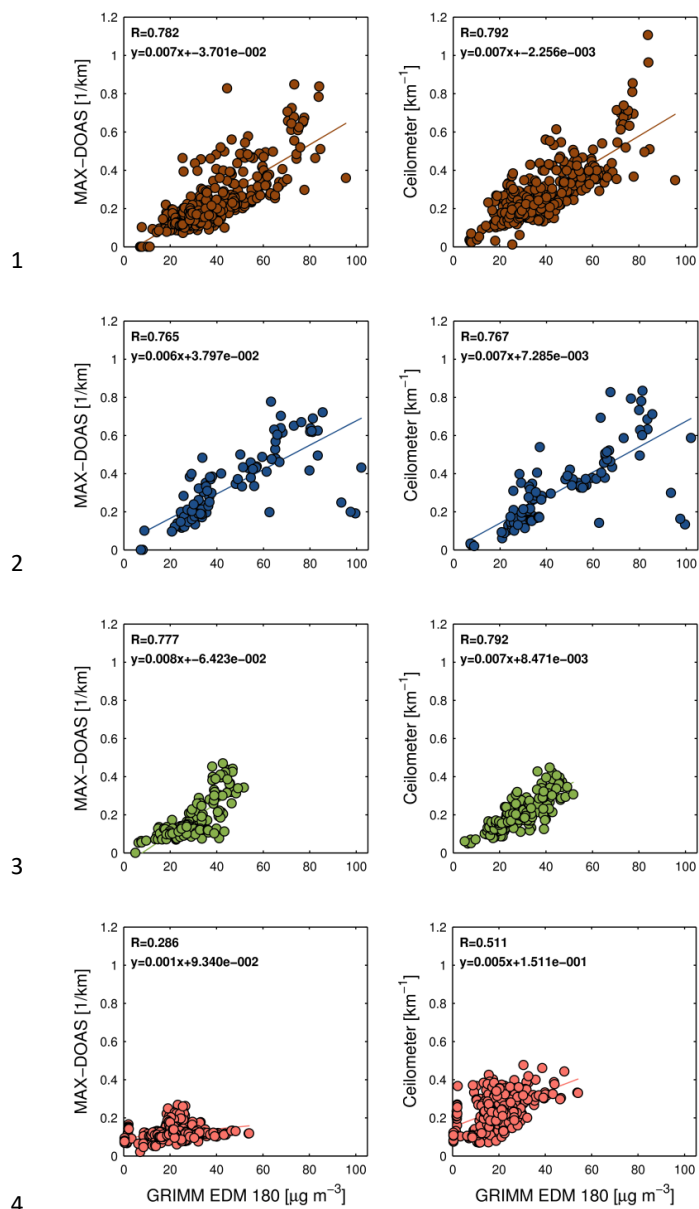
7

8

9



5 Figure 4. AOD scatterplots with their associated regression coefficients for the fall (brown), winter
 6 (blue), spring (green), and summer (red) seasons, illustrating the linear relationship of BOREAS
 7 AOD (obtained from BOKU MAX-DOAS, B, see Fig. 1) vs. AERONET AOD (obtained from sun
 8 photometer, B, see Fig. 1) in the UV (left panels) and visible (right panels) channels. Data of cloud-
 9 free days as defined in Sect. 2.2.1 between 1 September 2017 and 31 August 2019 are included.



5 Figure 5. AE scatterplots with their associated regression coefficients for the fall (brown), winter
 6 (blue), spring (green), and summer (red) seasons, illustrating the linear relationship of BOREAS
 7 (B, see Fig. 1) (left panels) and ceilometer (Z, see Fig. 1) (right panels) near-surface AE [1/km]
 8 retrieved in the UV channel vs. surface PM10 concentrations [µg m⁻³] from the in situ monitoring



1 station. Data of cloud-free days as defined in Sect. 2.2.1 between 1 September 2017 and 31 August
2 2019 are included in the plots.

3

4

5

6

7

8

9

10

11

12

13

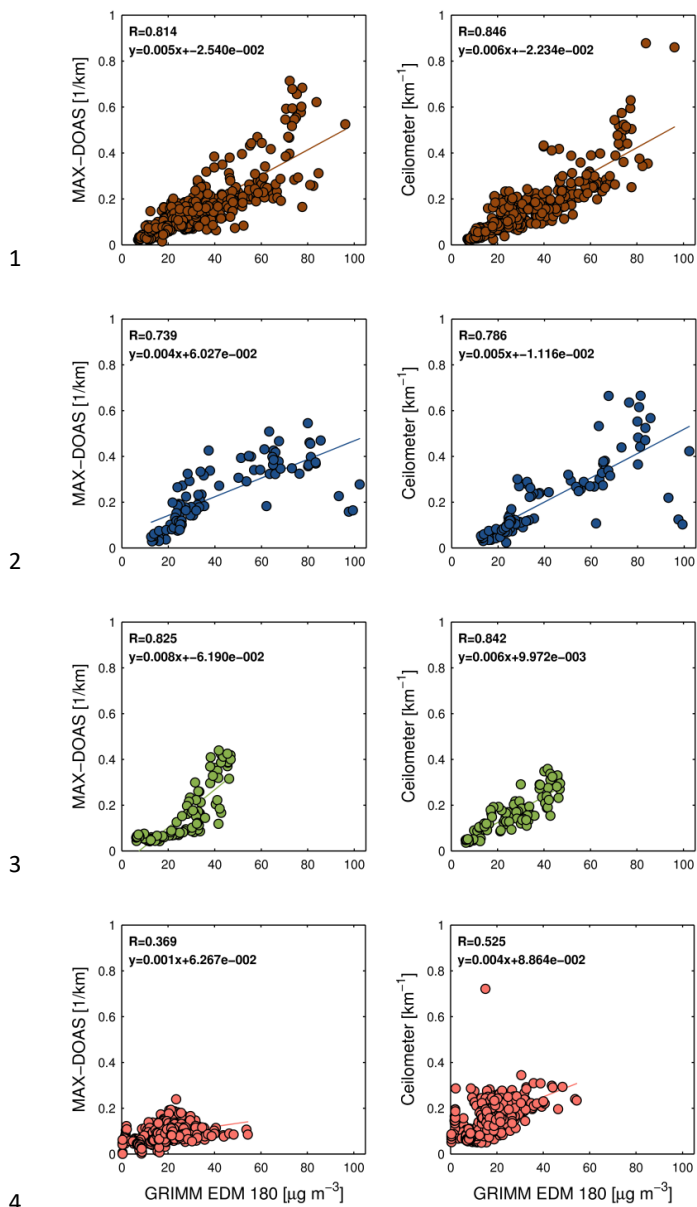
14

15

16

17

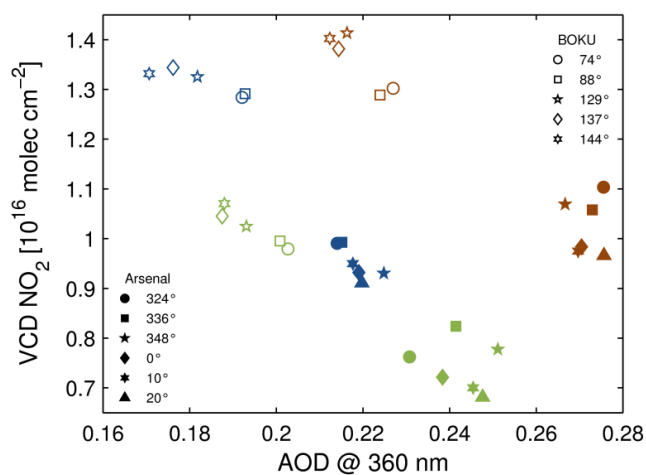
18



5 Figure 6. Same as Fig. 5, but for the visible channel.

6

7



1

2 Figure 7. Spatial variability of the BOREAS vertically-integrated profiling products AOD and
3 VCD NO₂, illustrated for the seasons fall (brown), winter (blue), and spring (green) as well as for
4 the different azimuth angles of the two MAX-DOAS instruments.

5

6

7

8

9

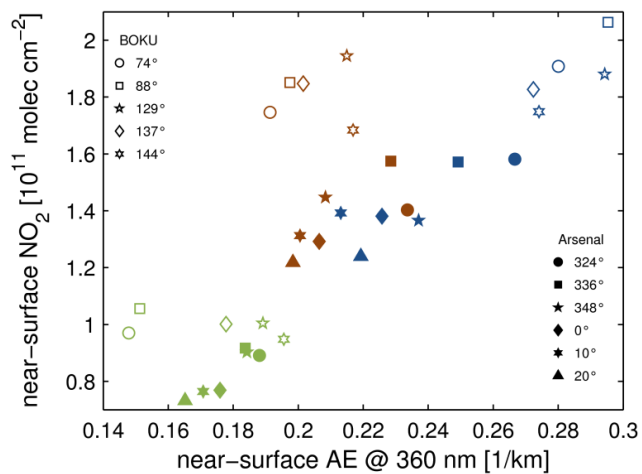
10

11

12

13

14



1

2 Figure 8. Same as Fig. 7, but for the near-surface retrieval products AE and NO₂.